Response of Porous Seabed to Nature Loadings: Waves and Currents

J. H. Ye[1] and D.-S. Jeng[2]

Abstract: In real ocean environments, currents generally exist simultaneously with ocean waves. However, the most previous investigations for the seabed response have only considered wave loading, ignoring currents. In this study, unlike previous studies, currents are included in the model of seabed response with waves, based on Biot's poroelastic dynamic theory ($u-p$ approximation). Numerical results reveal that the consideration of currents has significant effect on the seabed response. The opposing current is beneficial to prevent liquefaction, while the following current would worsen the stability of the seabed. The parametric studies indicate that the wave period, water depth, saturation, soil permeability, and thickness of the seabed significantly affect the seabed response under combined loading of waves and currents. The maximum relative difference of the pore pressure between the cases with currents (velocity is -2 m/s) and without currents $(p_{\text{current}}-p_{\text{nocurrent}})/p_0$ can reach up to 25% in both coarse and fine sand. The analysis of transient liquefaction in the fine sand seabed indicates that the maximum liquefaction depth increases with the following currents, but it decreases with the opposing current.
DOI: 10.1061/(ASCE)EM.1943-7889.0000356.

CE Database subject headings: Currents; Ocean waves; Sea floor; Porous media.

Author keywords: Currents; Waves; Seabed response; Porous seabed; Biot's theory; Liquefaction.

Introduction

It has been well documented that the ocean waves/currents exert dynamic pressures on a porous seabed. These dynamic variations will further cause the pore pressure, effective normal stresses, and shear stresses in a porous seabed. When the pore pressure in the seabed becomes excessive, the effective stresses between soil particles become zero; liquefaction will then occur and result in the collapse of marine structures built on the seabed. An inappropriate design and maintenance for the foundation of a marine structure would result in the failure of the structures. In recent engineering practice, some failures of marine structures because of the liquefaction or shear failure of the seabed have been reported (Zen et al. 1985; Lundgren et al. 1989).

Numerous investigations of the wave-induced transient dynamic response of the seabed under wave loading have been carried out based on Biot's poroelastic theory (Biot 1941; Biot 1956) since the 1970s. Among these, Yamamoto et al. (1978) derived an analytical solution for an isotropic, poroelastic, and infinite seabed by treating the pore water and seabed as a compressible and deformable medium. Later, Hsu and Jeng (1994) further extended the framework to an unsaturated, isotropic seabed with finite thickness under three-dimensional, short-crested wave loading. All these investigations were based on quasi-static Biot's consolidation equations. Jeng et al. (1999) and Jeng and Cha (2003) proposed analytical solutions of dynamic response for a poroelastic, isotropic seabed under wave loading based on the $u-p$ and full-dynamic approximations. A further extended version of the analytical solutions was proposed by Ulker et al. (2009), and the applicable range of all models is identified.

Numerical modeling is another efficient tool used to investigate the transient response of the seabed under wave loading. Thomas (1989, 1995) proposed a one-dimensional, finite-element model to investigate wave-induced soil response in a layered seabed. Later, Jeng and Lin (1996) further extended the model for a wave-induced soil response in a porous seabed with variable permeability and shear modulus along the burial depth. The seabed soil is unsaturated and hydraulically anisotropic, and subjected to a three-dimensional wave system. However, all these numerical models only considered wave loading. A detailed review of previous relevant research can be found in Jeng (2003).

In real ocean environments, the ocean waves and currents generally exist simultaneously. However, the aforementioned investigations have only considered wave loading without currents. Thus, how the ocean currents affect the wave-induced seabed response has not yet been examined. Actually, the pressure acting on the seabed is significantly different when there is a current in the flow field, according to the potential flow theory. Therefore, it is of interest to examine the influences of currents on the seabed response.

The effects of currents on the seabed response will be investigated numerically by adopting the $u-p$ approximation (Biot 1956; Zienkiewicz et al. 1980), in which the inertia terms of solid and pore fluid are both considered, as the governing equations for the porous seabed. The third-order approximation of nonlinear wave-current interaction (Hsu et al. 2009) is outlined first. The boundary value problem of wave-/current-seabed interactions is presented with a brief of the numerical scheme and the treatment of lateral boundary conditions. Verification of the proposed model is performed against the previous analytical solution and experimental data. Then, based on the numerical model, the effects of

[1]Postgraduate Student, Division of Civil Engineering, Univ. of Dundee, Dundee DD1 4HN, U.K.

[2]Professor, Division of Civil Engineering, Univ. of Dundee, Dundee DD1 4HN, U.K (corresponding author). E-mail: d.jeng@dundee.ac.uk; dongjeng@hotmail.com

Note. This manuscript was submitted on June 26, 2010; approved on November 17, 2011; published online on November 19, 2011. Discussion period open until November 1, 2012; separate discussions must be submitted for individual papers. This paper is part of the ***Journal of Engineering Mechanics***, Vol. 138, No. 6, June 1, 2012. ©ASCE, ISSN 0733-9399/2012/6-601–613/$25.00.

the current on the seabed response is investigated; a parametric study is carried out to investigate the effects of wave and soil characteristics on the seabed response, as well as the liquefaction under combined loading of nonlinear waves and currents.

Theoretical Formulations

Third-Order Approximation of Wave-Current Interactions

The coexistence of waves and currents in an offshore area is a common physical phenomenon, and their interaction is an important topic in the practices of coastal and ocean engineering. The presence of a current in a propagating wave will change the original characteristics of the wave. For example, the following current will elongate the wave length, and the opposing current will shorten the wave length. To obtain more accurate results of seabed response under combined wave and current loadings, the third-order solution of wave-current interactions is used to determine the dynamic wave pressures acting on the seabed. On the problem of the third-order wave-current interaction, some literature is available. The interaction between the linear wave and uniform current has been studied by Thomas (1981). Baddour and Song (1990b) further investigated the interaction of linear wave and collinear current. Later, Baddour and Song (1990a) further extended this problem to a third-order nonlinear wave and a uniform current. However, this analytical solution for the interaction between the third-order nonlinear wave and uniform current is not right because the third-order terms are not completed. Recently, gave out the complete form of analytical solutions for the problem of third-order nonlinear wave and uniform current interaction. Based on the work of Hsu et al. (1979), Jian et al. (2009) and Hsu et al. (2009) developed an analytical solution for the interaction between a gravity capillary short-crested wave and a uniform current. Here, the analytical solution proposed by Hsu et al. (2009) is adopted in order to apply the wave pressure on a porous seabed without marine structure.

The seawater is considered an incompressible and inviscid fluid, and the flow is irrotational. The flow field of seawater can be described by Laplace's equation

$$\nabla^2\phi = \frac{\partial^2\phi}{\partial x^2} + \frac{\partial^2\phi}{\partial z^2} = 0 \tag{1}$$

where ϕ = velocity potential. The horizontal and vertical velocity of the flow can be formulated as

$$u_f = -\frac{\partial\phi}{\partial x} \quad \text{and} \quad w_f = -\frac{\partial\phi}{\partial z} \tag{2}$$

where u_f and w_f = horizontal velocity and vertical velocity of the seawater in the flow field, respectively.

The dynamic and kinematic boundary conditions at the free surface are

$$-\frac{\partial\phi}{\partial t} + \frac{1}{2}(\phi_x^2 + \phi_z^2) + g\eta = C(t) \quad \text{at } z = d \tag{3}$$

$$\frac{\partial\eta}{\partial t} - \frac{\partial\phi}{\partial x}\frac{\partial\eta}{\partial x} + \frac{\partial\phi}{\partial z} = 0 \quad \text{at } z = d \tag{4}$$

where η = elevation of free surface relative to the static water level, and $C(t)$ = Bernoulli's constant. The bottom of the fluid domain is considered as impermeable

$$\frac{\partial\phi}{\partial z} = 0 \quad \text{at } z = 0 \tag{5}$$

Using the perturbation technique, Hsu et al. (2009) derived a third-order approximation for the wave-current interactions, which is summarized as follows:

$$\phi(x,z,t) = -U_0 x + \frac{Hg\ \cosh\lambda z}{2(U_0\lambda - \omega_0)\cosh\lambda d}\sin(\lambda x - \omega t) + \frac{3H^2\cosh 2\lambda z}{32\sinh^4\lambda d}(U_0\lambda - \omega_0)\sin 2(\lambda x - \omega t) + \frac{3\lambda^3 H^3}{512}\frac{(9 - 4\sinh^2\lambda d)\cosh 3\lambda z}{\sinh^7\lambda d}(U_0\lambda - \omega_0)\sin 3(\lambda x - \omega t) \tag{6}$$

$$\eta(x,t) = \frac{H}{2}\cos(\lambda x - \omega t) + \frac{\lambda H^2}{16}\frac{(3 + 2\sinh^2\lambda d)\cosh(\lambda d)}{\sinh^3\lambda d}\cos 2(\lambda x - \omega t) + \frac{\lambda^2 H^3}{512}\frac{(3 + 14\sinh^2\lambda d + 2\sinh^4\lambda d)}{\sinh^4\lambda d}\cos(\lambda x - \omega t) + \frac{\lambda^2 H^3}{512}\frac{3(9 + 24\sinh^2\lambda d + 24\sinh^4\lambda d + 8\sinh^6\lambda d)}{\sinh^6\lambda d}\cos 3(\lambda x - \omega t) \tag{7}$$

$$C(t) = \frac{U_0^2}{2} - \frac{H^2}{16}\frac{(\omega_0 - U_0\lambda)^2}{\sinh^2 kd} \tag{8}$$

where the H = wave height of the first-order wave, λ = wave number, d = water depth, U_0 = current velocity, g = gravity, and the dispersion relationship is given by

$$\omega = \omega_0 + (\lambda H)^2\omega_2 \tag{9}$$

where $\omega_0 = U_0\lambda + \sqrt{g\lambda\ \tanh\lambda d}$ and

$$\omega_2 = \frac{(9 + 8\sinh^2\lambda d + 8\sinh^4\lambda d)}{64\sinh^4\lambda d}(\omega_0 - U_0\lambda) \tag{10}$$

where the H = wave height of the first-order wave, λ = wave number, d = water depth, U_0 = current velocity, g = gravity, and the dispersion relationship is given by

$$\omega = \omega_0 + (\lambda H)^2\omega_2 \tag{11}$$

where $\omega_0 = U_0\lambda + \sqrt{g\lambda\ \tanh\lambda d}$ and

$$\omega_2 = \frac{(9 + 8\sinh^2\lambda d + 8\sinh^4\lambda d)}{64\sinh^4\lambda d}(\omega_0 - U_0\lambda) \tag{12}$$

The dynamic pressure acting on the seabed can be expressed

$$P_b(x,t) = \frac{\rho_f g H}{2\cosh\lambda d}\left[1 - \frac{\omega_2\lambda^2 H^2}{2(U_0\lambda - \omega_0)}\right]\cos(\lambda x - \omega t) + \frac{3\rho_f H^2}{8}\left\{\frac{\omega_0(\omega_0 - U_0\lambda)}{2\sinh^4(\lambda d)} - \frac{g\lambda}{3\sinh 2\lambda d}\right\}\cos 2(\lambda x - \omega t) + \frac{3\rho_f\lambda H^3\omega_0(\omega_0 - U_0\lambda)}{512}\frac{(9 - 4\sinh^2(\lambda d)}{\sinh^7\lambda d}\cos 3(\lambda x - \omega t) \tag{13}$$

where ρ_f = density of seawater. When there is no current in the wave ($U_0 = 0$ m/s), the above third-order solution can be reduced to the classic form of the solution of the third-order nonlinear wave.

The presence of a current in a wave propagating on the seabed will change the original wave characteristics because of the interactions between the currents and waves. The effect of a uniform current on the wave characteristics (wave number, wave length, maximum pressure, and wave celerity) is illustrated in Fig. 1. The following current (i.e., the current in the same direction of the wave propagation) could significantly elongate the length of the wave, and make the maximum pressure acting on the seabed increase greatly. On the other hand, the opposing current could significantly shorten the length of the wave, and make the maximum pressure acting on the seabed decrease. The effect of a uniform current on the wave characteristics determined by the linear theory of wave-current interaction is also plotted in Fig. 1. The linear theory overestimates the wave number, but underestimates the wave length. In particular, the linear theory of wave-current interaction significantly underestimates the maximum pressure acting on the seabed relative to that determined by the third-order theory.

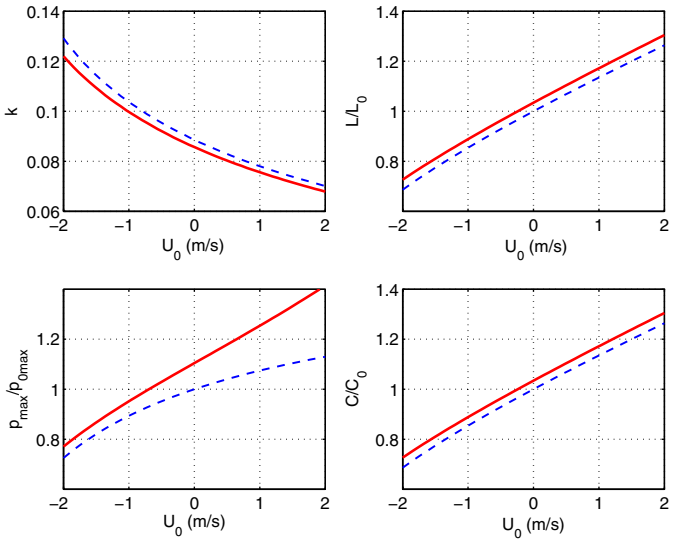

Fig. 1. Effect of the current on the wave number k, wave length L, induced maximum pressure acting on the seabed $p_{\max}$, and the wave celerity C ($H = 3.0$ m, $d = 10$ m, $t = 8.0$ s); L_0, $(p_0)_{\max}$, and C_0 are the wave length, maximum pressure, and wave celerity determined by the linear wave theory without a current (i.e., $U_0 = 0$ m/s), respectively; solid lines = third-order theory, dashed lines = linear theory

Seabed Model

The problem considered is illustrated in Fig. 2, where the seabed is treated as an elastic, isotropic, and homogeneous porous medium. The relative displacements of soil particle to pore fluid are ignored, and then the porous flow in a seabed is governed by the following equations (Zienkiewicz et al. 1980), which is the so-called $u - p$ approximation:

$$\frac{\partial\sigma'_x}{\partial x} + \frac{\partial\tau_{xz}}{\partial z} = -\frac{\partial p}{\partial x} + \rho\frac{\partial^2 u}{\partial t^2} \tag{14}$$

$$\frac{\partial\tau_{xz}}{\partial x} + \frac{\partial\sigma'_z}{\partial z} + \rho g = -\frac{\partial p}{\partial z} + \rho\frac{\partial^2 w}{\partial t^2} \tag{15}$$

$$k\nabla^2 p - \gamma_w n\beta\frac{\partial p}{\partial t} + k\rho_f\frac{\partial^2\epsilon}{\partial t^2} = \gamma_w\frac{\partial\epsilon}{\partial t} \tag{16}$$

where (u, w) = the soil displacements in the horizontal and vertical directions, respectively; n = soil porosity; σ'_x and σ'_z = effective normal stresses in the horizontal and vertical directions, respectively; τ_{xz} = shear stress; p = the pore water pressure; $\rho = \rho_f n + \rho_s(1 - n)$ = the average density of the porous seabed; ρ_f = the fluid density; ρ_s = solid density; k = the Darcy's permeability; g = the gravitational acceleration; and ϵ = the volumetric strain. In Eq. (15), the compressibility of pore fluid (β) and the volume strain (ϵ) are defined as

$$\beta = \left(\frac{1}{K_f} + \frac{1 - S_r}{p_{w0}}\right), \quad \text{and} \quad \varepsilon = \frac{\partial u}{\partial x} + \frac{\partial w}{\partial z} \tag{17}$$

where S_r = the degree of saturation of the seabed, p_{w0} = the absolute static pressure, and K_f = the bulk modulus of pore water ($K_f = 2^9$ N/m^2, Yamamoto et al. 1978).

The linear poroelastic constitutive model is adopted for the transient wave-induced seabed response. Under the condition of plane strain, the stress-strain relationship is given as

$$\begin{bmatrix}\sigma'_x\\ \sigma'_z\\ \tau_{xz}\end{bmatrix} = \frac{E}{(1+\nu)(1-2\nu)}\begin{bmatrix}1-\nu & \nu & 0\\ \nu & 1-\nu & 0\\ 0 & 0 & \frac{1-2\nu}{2}\end{bmatrix}\begin{bmatrix}\frac{\partial u}{\partial x}\\ \frac{\partial w}{\partial z}\\ \frac{\partial u}{\partial z} + \frac{\partial w}{\partial x}\end{bmatrix} \tag{18}$$

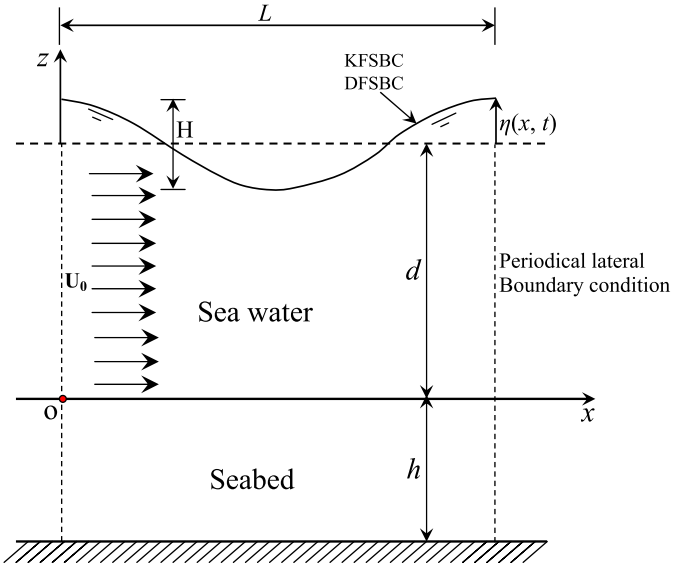

Fig. 2. Sketch of wave-/current-seabed interaction

where E = the elastic modulus; ν = Poisson's ratio; and u and w = the horizontal and vertical soil displacements, respectively.

To solve the governing Eqs. (14) and (16), several boundary conditions were applied. First, the bottom of the seabed is considered rigid and impermeable. Therefore, there is no displacement and vertical flow at this bottom (note that the x-axis coincides with the seabed surface when studying the seabed response).

$$u = w = 0 \quad \text{and} \quad \frac{\partial p}{\partial z} = 0 \quad \text{at } z = -h \tag{19}$$

Second, the boundary conditions along the surface of the seabed can be expressed as

$$p(x, z = 0, t) = P_b(x, t) \quad \text{and} \quad \tau_{xz} = 0 \quad \text{at } z = 0 \tag{20}$$

The boundary condition [Eq. (20)] implies that this approach does not consider the damping because of the porous seabed. It is a one-way coupling (or a so-called weak coupling), rather than a two-way coupling (i.e., full coupling) process. A simple analytical approach proposed by Jeng (2001) is adopted to examine the effects of seabed characteristics on wave characteristics. In Jeng's (2001) paper, the influence of the seabed on the wave parameters, such as wave height and wave length, has been shown. However, the main focus is the effect of the combined wave and current loadings on the seabed response. Thus, the one-way coupling (weak coupling) is used, which has been widely used in previous literature. As shown in a subsequent section, this model can provide reasonable prediction of the seabed response in comparison with experimental data (Lu 2005).

Numerical Model and Treatment of Lateral Boundary Conditions

The finite-element model (SWANDYNE Dynamic Version II), originally developed by Chan (1988) for the soil response under earthquake loading, is adopted for wave loading. A wave module [Cornell Breaking Waves and Structure (COBRAS)] used to apply wave loading to the porous seabed is developed and integrated to SWANDYNE II to form part of the numerical model Porous Models for Wave-Seabed-Structure Interaction, version II (PORO-WSSI II). Details of the generalized finite-element method (FEM) formulations are available in Jeng and Ou (2010).

In this section, we present the treatment of the lateral boundaries that was not available in Jeng and Ou (2010). Generally speaking, at the two lateral boundaries, the horizontal and vertical displacements, and the flow out/in of the pore water do not vanish. The principle of repeatability (Zienkiewicz and Scott 1972) has been employed to handle periodic problems, such as the wave-seabed interaction (Jeng et al. 2000). However, the periodic boundary condition requires that the length of the computational domain must be an integer of the length of the wave. Furthermore, the principle of the periodic condition is applied to the problems of neither nonperiodic loading nor with a marine structure.

An alternative method is to use a large computational domain and fix both the lateral conditions in the horizontal direction, rather than applying the periodic boundary condition. This method is based on the assumption that the effects of the fixed lateral boundaries are only limited to the region near the lateral boundaries. In the region far away from the lateral boundaries, the effect of the fixed lateral boundaries will disappear. The computational results are the same when the periodic boundary condition is applied to the lateral sides of the computational domain whose length is equal to the length of the wave.

In principle, a larger computational domain will reduce the effect of the fixed lateral boundaries. However, a large computation domain will require huge computational time and larger memory. Therefore, the length of the computation domain is chosen as 2.0–3.5 times the maximum wave length adopted in all cases. Herein, we will investigate the effects of lateral boundaries on the soil response in the region we are interested in. A numerical example, with the input data given in Table 1, is illustrated in Fig. 3. In the numerical example, we consider a computational domain of 250-m long, which is about 3.4 times the wave length ($L = 73.3$ m). In Fig. 3, both results from the present model (fixed boundaries) and the previous model with the principle of repeatability (Jeng et al. 2000) are included for comparison.

The results presented in Fig. 3 of three sections at $x = 50$ m, 125 m, and 200 m are considered. As shown in Figs. 3(a) and 3(c), the pore pressure and vertical effective stress are basically identical for both models; however, significant differences between the two models are observed for the horizontal effective stress and shear stress. This indicates that the method of a fixed lateral boundary may not be applicable at position $x = 50$ m and $x = 200$ m. In contrast, Fig. 3(b) shows the comparison of the seabed response at the midline $x = 125$ m for both treatments of lateral boundary conditions, and indicates that the effect of the fixed lateral boundaries disappears completely at the region far away from the fixed lateral boundaries. Based on this numerical exercise, the proposed treatment method for the lateral boundaries is acceptable under the condition of a sufficiently large computational domain. Therefore, the same mesh system being used for all cases in which different wave lengths are involved is feasible, and the accurate results could be obtained at the region far away from the fixed lateral boundaries, which is our main investigation zone.

Numerous numerical tests for the use of the proposed treatment and the concept of repeating loading have been carried out. A representative graph (Fig. 4) is shown here to demonstrate the

Table 1. Input Data for Numerical Examples

Wave characteristics	Value	Soil characteristics	Value
Wave period (T)	8.0 s	Permeability (k)	10^{-2} m/s (coarse sand) 10^{-4} m/s (fine sand)
Wave height (H)	2.0 m	Porosity (n)	0.3 (coarse sand) 0.2 (fine sand)
Water depth (d)	20 m	Shear modulus (G)	10^7 N/m^2
Current (U_0)	1 m/s (following current) −1 m/s (opposing current)	Poisson's ratio (μ)	1/3
		Saturation (S_r)	0.98
		Thickness (h)	30 m

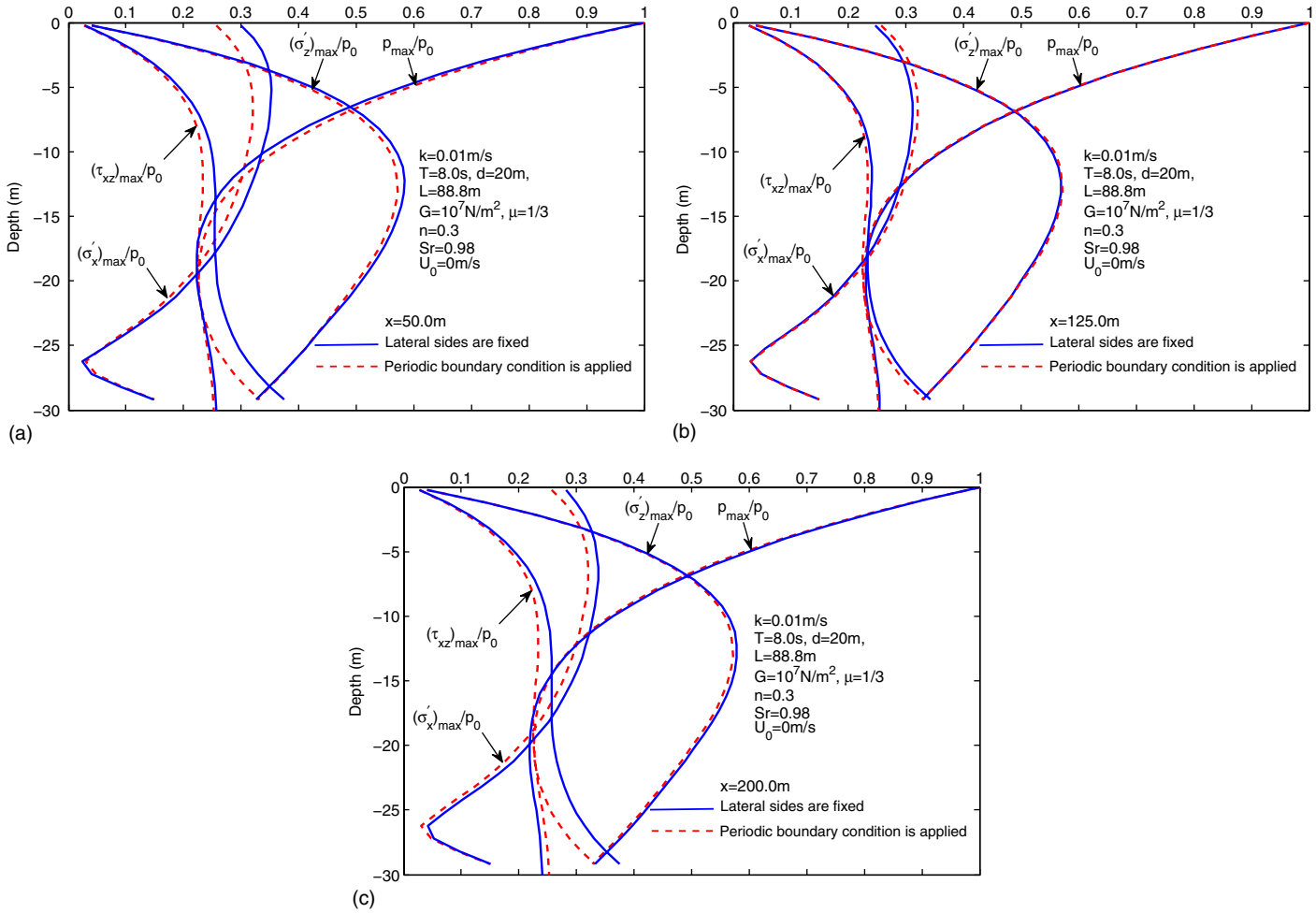

Fig. 3. Comparison of the seabed response under the same wave loading at $x = 50$ m, 125 m, and 200 m between the case in which the lateral boundaries are fixed and the case in which the periodic boundary condition is applied

effect range of the fixed lateral sides. The vertical axis is the relative difference of the wave induced σ'_x at depth $z = -5$ m between the results determined by adopting the fixed lateral boundary and periodic boundary. The horizontal axis is the distance to the fixed lateral sides (normalized by wave length L). Herein, σ'_x is chosen as the representative variable because the effect of the fixed lateral sides on wave induced σ'_x is most obvious in the upper seabed, which can be observed in Fig. 3. As illustrated in Fig. 4, the effect of the fixed lateral sides basically could disappear if the distance to the lateral fixed sides is greater than one wave length.

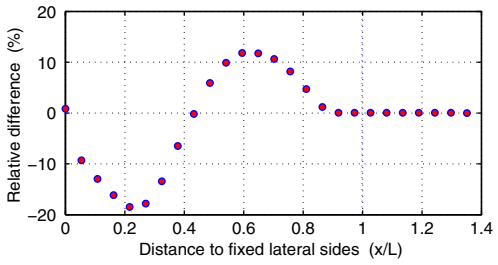

Fig. 4. Relative difference of wave induced maximum σ'_x at depth $z = -5$ m between the results determined by adopting the fixed lateral boundary and periodic boundary versus the distance to the fixed lateral sides (normalized by wave length L); $H = 3.0$ m, $T = 8.0$ s, $d = 10.0$ m, and $U_0 = 1.0$ m/s

Verifications

It is important and necessary to validate the proposed numerical model PORO-WSSI II against existing models for several special cases. Because neither experimental nor theoretical work for the seabed response under a combined wave and current loading is available, we can only compare our model with the previous work without currents. To verify the numerical model, the model is compared with the analytical solution (Hsu and Jeng 1994) and the experimental data conducted by Lu (2005).

The numerical results of the maximum values of wave-induced pore pressure and effective stresses in unsaturated coarse/fine sand (the degree of saturation = 98%) are shown in Fig. 5. The results of the analytical solution (Hsu and Jeng 1994) are also plotted in Fig. 5. From Figs. 5(a) and 5(b), the results of the numerical model overall agrees well with the analytical solution. The minor differences between the two models are that the analytical solution is based on quasi-static soil behavior and the present numerical model is based on the $u - p$ approximation.

Lu (2005) conducted a series of laboratory experiments on the dynamic response of the sandbed to the waves propagating on it in a wave flume, which is 60-m long, 1.5-m wide, and 1.8-m high. The waves generated in the wave flume include regular and cnoidal

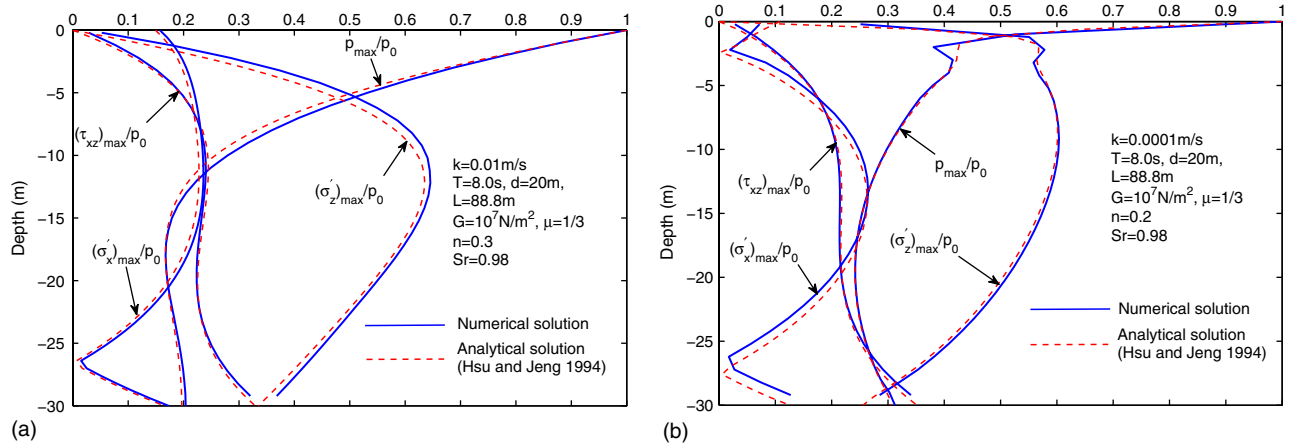

Fig. 5. Vertical distributions of the wave-induced soil response in (a) coarse sand and (b) fine sand ($S_r = 0.98$)

waves; the seabed is coarse sand. The pore pressure at the four points on the midline of the sandbed is monitored in the experiments. Because only regular waves were considered, only the experimental data of the regular waves for validation were used. Detailed information of the experiment setup is available in Lu (2005). The properties of the coarse sand provided by Lu (2005) are as follows: shear modulus $G10^7$ N/m^2, Poisson's ratio $\mu = 0.3$, permeability $k = 10^{-3}$ m/s, porosity $n = 0.3893$, mean size of sand particles $d_{50} = 0.44$ mm, and saturation S_r = 98%. The wave characteristics of the regular and cnoidal waves are as follows: $H = 14$ cm, $d = 0.4$ m, $T = 1.2$ s and $H = 14$ cm, $d = 0.3$ m, $T = 2.0$ s, respectively.

The comparisons of the regular wave-induced dynamic pore pressure at the four points on the midline of the sandbed between the numerical results and the experimental data are shown in Fig. 6. Fig. 6 shows that the results predicted by the numerical model overall agree well with the experimental data provided by Lu (2005).

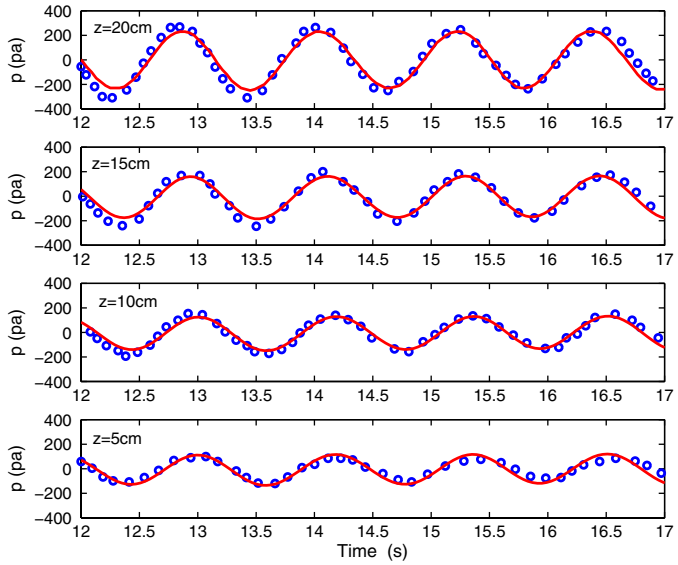

Fig. 6. Comparisons of wave induced dynamic pore pressure on the midline of the sandbed between the numerical results and the experimental data in Lu's (2005) experiments; lines = numerical results, circles = experimental data

Results and Discussions

The main objective is to examine the influence of current on the seabed response, including the pore pressures, effective stresses, shear stresses, and liquefaction potential. In this section, we first examine the effect of ocean currents on the seabed dynamic response through comparison with the case without currents (i.e., wave only). Four cases (two for following currents and another two for opposing currents) in coarse and fine sand are considered. The soil characteristics used in the numerical examples are given in Table 1. The wave characteristics used are in the range of nonlinear wave ($H = 3.0$ m, $T = 8.0$ s, $d = 10.0$ m). In these examples, the length of the computation domain is 250 m for all four cases, which is 2.7 times the maximum wave length involved in following currents; and the current velocity is chosen as 1 m/s (the following current) and -1 m/s (the opposing current).

Effects of Currents

In this section, we compare the seabed response for the cases under waves loading with and without currents. Fig. 7 illustrates the vertical distributions of the seabed response under the wave and following current ($U_0 = 1$ m/s) loading at $x = 125$ m in both coarse and fine sand. Because of the fact that the absolute value of maximum and minimum dynamic response in the seabed is greatly different under highly nonlinear wave loading, the maximum and minimum dynamic responses in the seabed are compared, with their corresponding values when $U_0 = 0$ m/s. In Fig. 7, all seabed response variables are normalized by the maximum dynamic wave pressure along the seabed surface without a current, that is, $(p_0)_{max}$, $|(p_0)_{min}|$, given in Eq. (13) when $U_0 = 0$ m/s. In Fig. 7 the effect of ocean currents on the seabed response is significant in both coarse and fine sand. If a following current exists in the wave field, the magnitudes of the maximum/minimum seabed response, including pore pressure and effective stresses, are basically greater than without currents. For the maximum/minimum shear stress in the seabed, both cases are almost identical in the upper part of the seabed. In the lower part of the seabed, the magnitude of shear stress is greater when there is a following current. In coarse sand, the maximum relative difference between the two cases with/without currents can be up to 15% for maximum/minimum pore pressure, and 10% for $(\sigma'_z)_{max/min}$, 5% for $(\sigma'_x)_{max/min}$, and 10% for the shear stress $(\tau_{xz})_{max/min}$. Although the magnitude of the relative difference of the seabed response between the two cases is not large, the absolute difference is huge

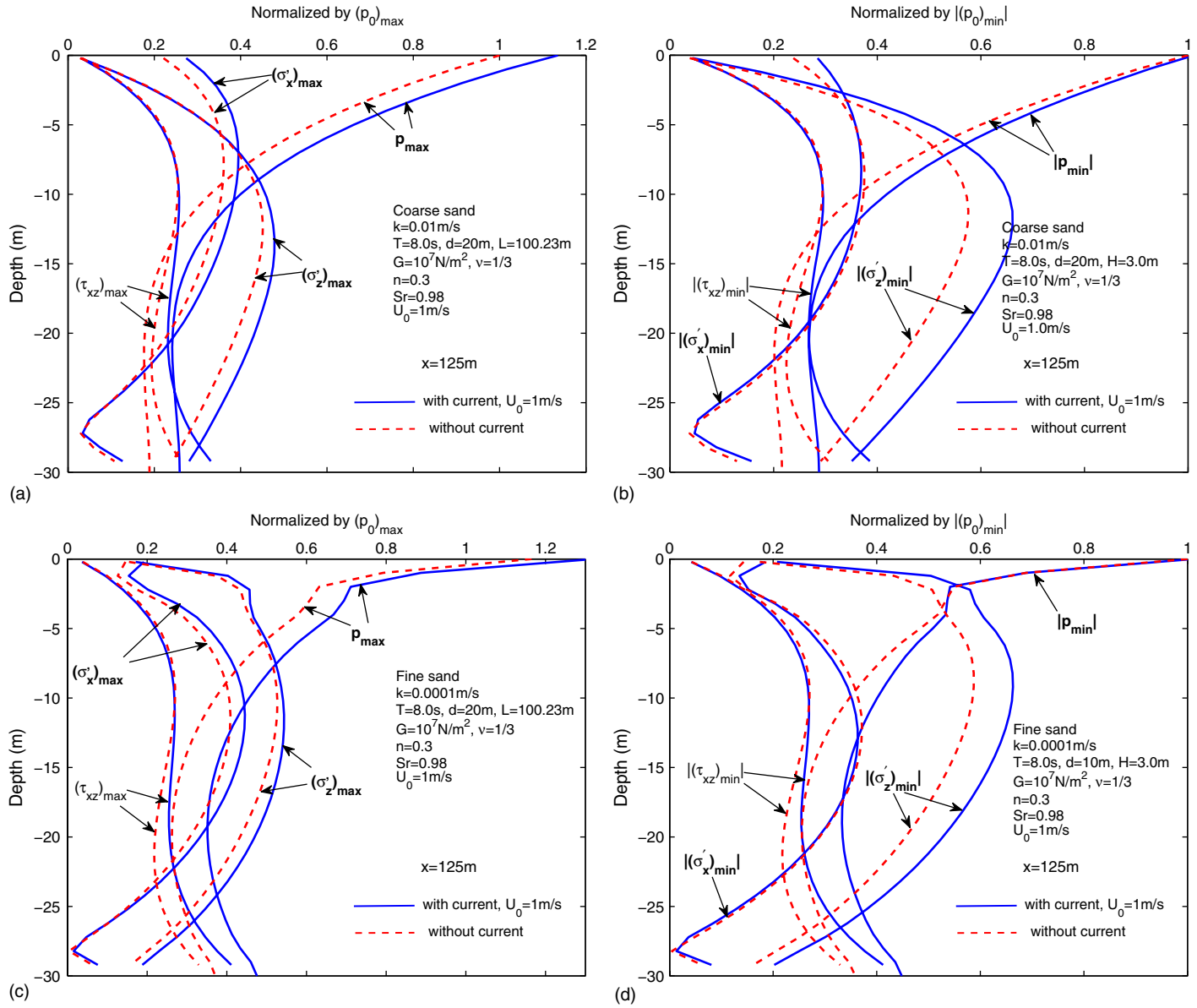

Fig. 7. Vertical distributions of the seabed response under the wave and following current ($U_0 = 1$ m/s) loading in (a) coarse sand and (b) fine sand

because all quantities have been normalized by a great value, $(p_0)_{max}$ or $|(p_0)_{min}|$. These results indicate that the seabed instability (e.g., liquefaction) is more likely to occur (to be discussed further in a subsequent section) if the ocean wave and following current coexist simultaneously regardless of the soil type.

Fig. 8 further presents the vertical distributions of the maximum/minimum seabed response under nonlinear wave and opposing current loading at $x = 125$ m in coarse and fine sand when the current velocity $U_0 = -1$ m/s. The effect of the opposing current on the seabed response is also significant, as shown in Fig. 8. However, the seabed response will be smaller than the case without currents, which may reduce the potential of seabed instability.

Parametric Study

Effect of the Magnitude of the Current Velocity

In the ocean environments, the velocity of the ocean current generally is less than 2 m/s except for some special situations, such as a storm or tsunami. Therefore, the current velocities used in the numerical examples are 0.5 m/s, 1 m/s, 1.5 m/s, and 2.0 m/s. Additionally, the following current and opposing current with the four magnitudes of velocity are investigated to show the effects of the flow direction of currents.

Figs. 9 and 10 show the vertical distributions of the relative difference of the seabed response under nonlinear wave-current loading in coarse and fine sand for the different current velocity U_0. Here, all relative differences are normalized by $p_0 = (p_0)_{max} + |(p_0)_{min}|$, which is the sum of the maximum wave pressure (induced by the wave crest) and the absolute value of the minimum wave pressure (induced by the wave trough) when $U_0 = 0$ m/s. In Figs. 9 and 10, it is observed that the response of the seabed, including pore pressure, effective stresses and shear stress, under wave, and following current loading is greater than those under wave loading only, and the seabed response under wave and opposing current loading is smaller than those under wave loading only. The greater the magnitude of the current velocity, the greater the relative difference relative to that condition when $U_0 = 0$ m/s. The maximum relative differences of the pore pressure between the two conditions $U_0 = -2$ m/s and $U_0 = 0$ m/s can reach

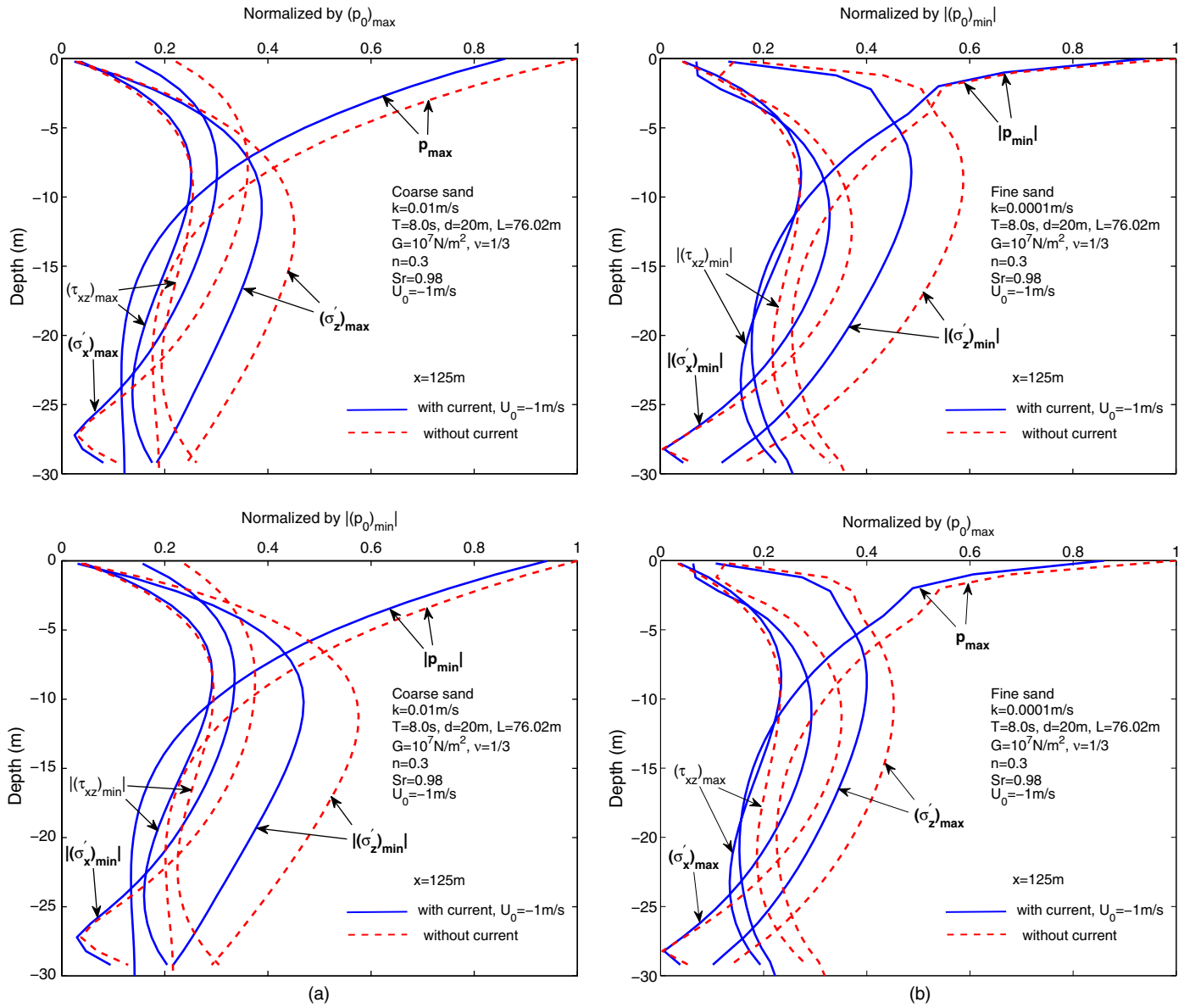

Fig. 8. Vertical distributions of the seabed response under the wave and opposing current ($U_0 = -1$ m/s) loading in (a) coarse sand and (b) fine sand

25%, as seen in Fig. 9(a). It is also observed that the relative differences of the seabed response under nonlinear waves and opposing currents are overall greater than that of the seabed response under nonlinear waves and following currents even when the magnitude of the current velocity is the same, for example, $U_0 = -2$ m/s and $U_0 = 2$ m/s.

If there is a current in the wave field, the maximum relative difference of vertical effective stress (σ'_z) occurs at the middle part of the seabed in coarse sand, while it occurs at the region near the seabed surface in fine sand (see Figs. 9 and 10). The maximum relative difference of (τ_{xz}) occurs at the impermeable bottom of the seabed in both coarse and fine sand.

Based on the numerical examples presented, the combined wave and following current loading will enhance the potential of seabed instability, such as liquefaction, while the opposing current is beneficial to prevent the seabed from liquefaction or shear failure. Once the liquefaction occurs, the maximum depth of liquefaction would be deeper than the situation in which there is no current. Therefore, the following current will aggravate the instability of the seabed. It is a potential risk for marine structures located on the seabed.

Effect of Wave Characteristics

In this section, we further investigate the effects of wave parameters on the relative differences of pore pressure $(p_{\text{current}} - p_{\text{no-current}})/p_0$. Two wave characteristics, wave period and water depth, are examined here.

As shown in Fig. 11, the effect of the following current on the seabed response is significant for a short period wave in the upper part of the seabed. For example, the maximum relative difference is up to 25% at the surface of the seabed when ($T = 5.0$ s); while, the effect of the following current on the seabed response for a large period wave ($T = 12.0$ s) is not as significant. However, it is interesting to point out that the effect of the following current on the seabed response for a medium period wave ($T = 8.0$ s) is not in the range of relative differences of short period and large period waves. The relative difference is smallest in the region nearest to the seabed surface for a medium period wave, and

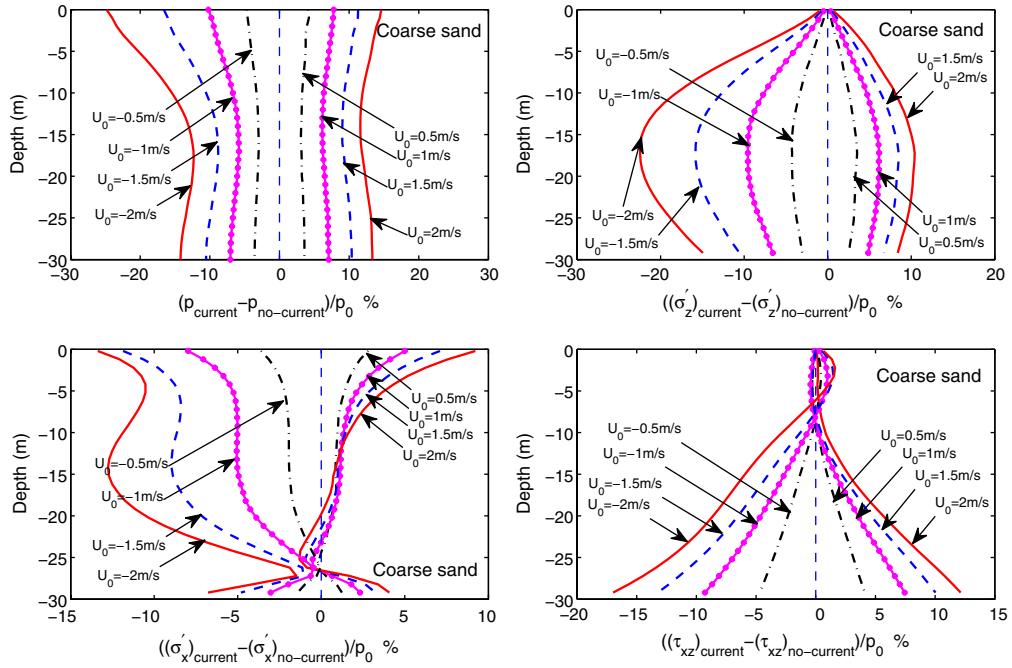

Fig. 9. Vertical distributions of the relative differences of the wave-current induced seabed response in coarse sand for different U_0

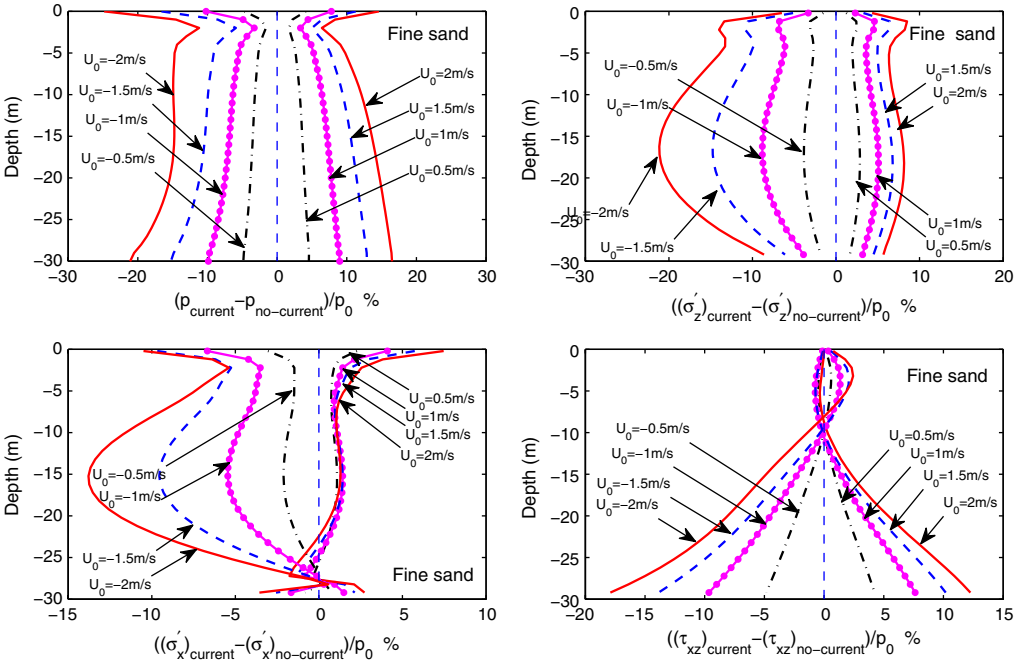

Fig. 10. Vertical distributions of the relative differences of wave-current induced seabed response in fine sand for different U_0

the relative difference increases gradually along the seabed depth. At the bottom of the seabed, the relative difference is the greatest for a medium period wave.

Fig. 12 illustrates the vertical distributions of the relative difference of pore pressure versus soil depth in coarse and fine sand for various water depths. The water depth has a significant effect on wave-current induced pore pressure in the seabed. The deeper the water depth, the more significant the effect of the following current on the seabed response in both coarse and fine sand. When a wave is propagating in deep water, the current-induced pressure accounts for a major proportion of the whole wave-current induced pressure acting on the seabed surface. Therefore, the effect of the current is relatively significant.

Effect of Soil Characteristics

Soil characteristics are another important parameter that must be considered in the analysis of seabed instability. Among these, three parameters are examined. The parameters are the following: the degree of saturation, seabed thickness, and soil type (in term of soil permeability).

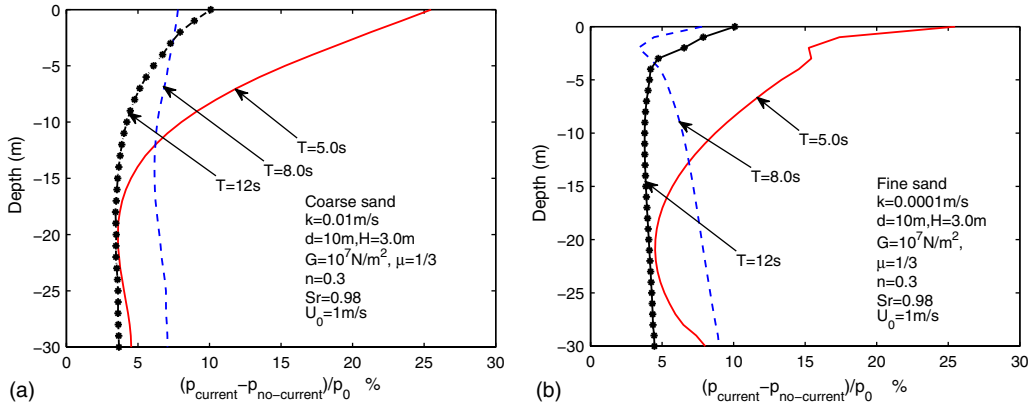

Fig. 11. Vertical distributions of the relative difference of pore pressure, $(p_{\text{current}} - p_{\text{no-current}})/p_0$, for various wave periods

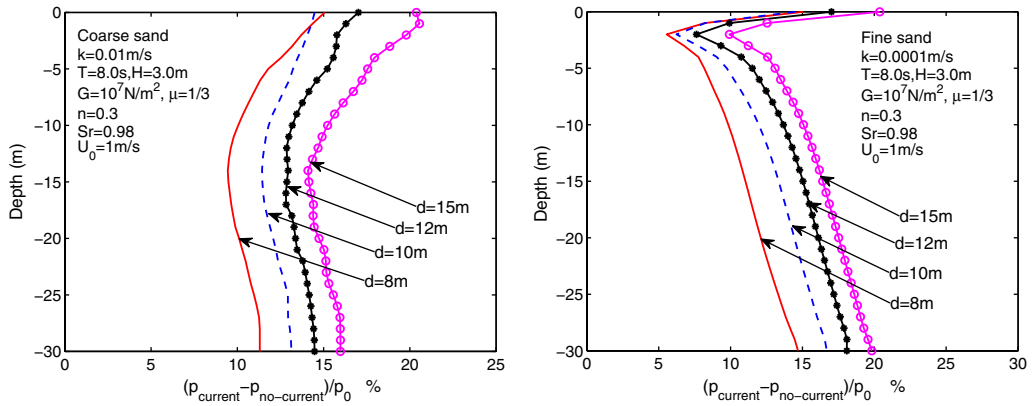

Fig. 12. Vertical distributions of the relative difference of pore pressure, $(p_{\text{current}} - p_{\text{no-current}})/p_0$, for various water depth

The degree of saturation has been recognized as one of the dominant factors in the evaluation of wave-induced seabed response. The compressibility of pore water in the seabed is mainly dependent of the degree of saturation. It is reported that the in-site degree of saturation of marine sediments normally lies in the range of 85%–100% (Esrig and Kirby 1977; Pietruszczak and Pande 1996). Three representative degrees of saturation are chosen to investigate the effect of the current on the seabed response in a seabed with a different saturation. They are 95%, 98%, and 100%, respectively.

Fig. 13 presents the vertical distributions of the relative difference of dynamic pore pressure, $(p_{\text{current}} - p_{\text{no-current}})/p_0$, in coarse and fine sand for various degrees of saturation. In Fig. 13, the degree of saturation has significant effects on the wave-current induced pore pressure both in coarse and fine sand. The relative difference between the wave-current induced pore pressure and the wave induced pore pressure (without current) increases as the degree of saturation increases. This means that the effect of the current is most significant in a fully saturated seabed.

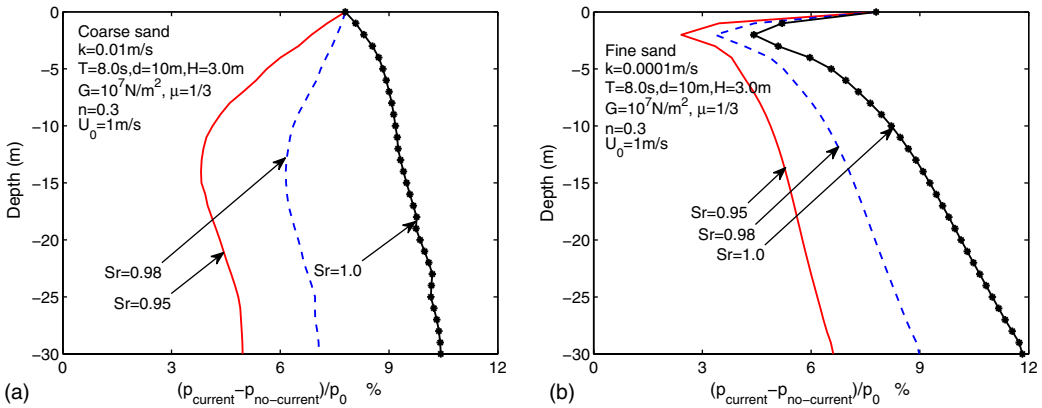

Fig. 13. Vertical distributions of the relative difference of pore pressure, $(p_{\text{current}} - p_{\text{no-current}})/p_0$, for various degrees of saturation

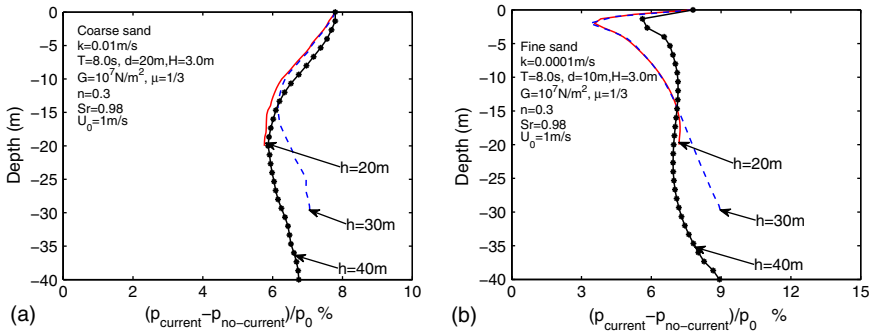

Fig. 14. Vertical distributions of the relative difference of pore pressure, $(p_{\text{current}} - p_{\text{no-current}})/p_0$, for various seabed thickness

The maximum relative difference occurs at the impermeable bottom of the seabed both in coarse and fine sand, if the seabed is fully saturated.

The thickness of the seabed is another factor that would affect the effect of currents on the seabed response. Fig. 14 illustrates the vertical distributions of the relative difference of pore pressure, $(p_{\text{current}} - p_{\text{no-current}})/p_0$, in coarse and fine sand for various seabed thickness. From Fig. 14, it is found that the effect of the following current ($U_0 = 1$ m/s) on the seabed response is almost the same at the top of the seabed (0 to −15 m) in coarse sand. In the lower part of the seabed (less than −20 m), the relative difference of the pore pressure is greater in a thin seabed. In fine sand, the situation is different in the upper part of the seabed. The relative difference of pore pressure is greatest in a thick seabed.

In addition to the degree of saturation and seabed thickness, soil permeability is another important factor in the analysis of wave/current induced soil response. Based on the results presented in Figs. 11–14, the influence of currents on the seabed response is more significant in fine sand than compared with coarse sand.

Liquefaction of Seabed under Combined Nonlinear Wave and Current Loading

It is well known that the porous seabed would liquefy under wave loading because of the buildup of excess pore pressure in the seabed. To investigate the liquefaction properties in the seabed under combined nonlinear wave and current loading, the liquefaction criterion proposed by Okusa (1985) are adopted. It is expressed as

$$-(\gamma_s - \gamma_w)z \leq \sigma'_z \tag{21}$$

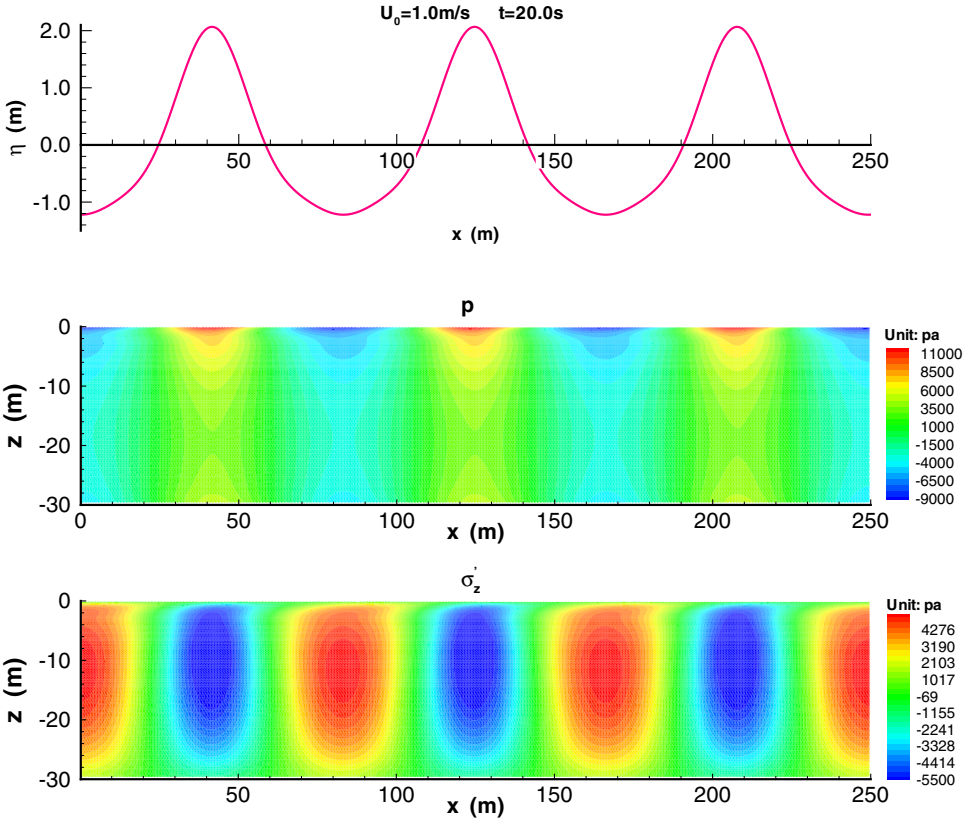

Fig. 15. Free surface of the third-order wave, and the distribution of wave-induced dynamic pore pressure and vertical effective stress σ'_z in fine sand at time $t = 20.0$ s ($U_0 = 1$ m/s)

where the γ_s = saturation unit weight of the seabed soil, γ_w = unit weight of water, and σ'_z = wave induced vertical dynamic effective stress. Actually, the liquefaction criterion [Eq. (21)] means that the seabed will liquefy if the wave induced vertical dynamic effective stress σ'_z (note that the compressive stress is negative) is equal to or greater than the original vertical effective stress $-(\gamma_s - \gamma_w)z$. The dynamic effective stresses are determined through the following three steps: (1) calculating the consolidation state of the seabed under the static water pressure, (2) calculating the full effective stresses state of the seabed under full water pressure including static pressure and wave-induced dynamic pressure, and (3) the dynamic effective stresses are determined by subtracting the effective stresses of the consolidation state from the full effective stresses.

Fig. 15 shows the elevation of the free surface of third-order stokes wave with a following current at time $t = 20.0$ s ($U_0 = 1$ m/s), and the distribution of the corresponding dynamic pore pressure p and vertical effective stress σ'_z in fine sand. As illustrated in Fig. 15, in the region in the seabed under the wave crest, the dynamic pore pressure is positive, and the dynamic vertical effective stress is compressive. While, in the region in the seabed under the wave trough, the dynamic pore pressure is negative, and the dynamic vertical effective stress is tensile. Therefore, the seabed under the wave trough is most likely to be liquefied. Fig. 16 shows the liquefied zones in the seabed under a nonlinear wave loading at time $t = 20.0$ s. In Fig. 16, all liquefied zones in the seabed are located in the regions near the wave troughs because the tensile vertical effective stress is generated, and only the upper part of seabed could be liquefied.

The transient liquefied zones move in the seabed, accompanying the movement of the third-order progressive wave. Therefore, there is no place that is always in the liquefied state if the elastic model is used for the porous seabed. Fig. 17(a) illustrates the variation process of liquefied depth in the fine sand seabed in time domain $x = 125$ m under nonlinear wave and current ($U_0 = -1$ m/s, 0 m/s, and 1 m/s) loading. As shown in Fig. 17(a), the maximum liquefied depth in the seabed is 1.16 m, 0.98 m, and 0.58 m when the velocity of the current U_0 is 1 m/s, 0 m/s, and -1 m/s, respectively. Relative to the condition without a current, the following current $U_0 = 1$ m/s makes the maximum liquefied depth increase 18%, while the opposing current makes the maximum liquefied depth decrease 57%. From this result, it is found that the following current makes the liquefied zone in the seabed become larger than when there is no current; and the opposing current is beneficial to prevent the seabed from liquefying. Fig. 17(b) shows the relationship between the maximum liquefied depth and the current velocity under condition $H = 3.0$ m, $d = 10.0$ m, $T = 8.0$ s. In Fig. 17(b), the following current makes the fine sand seabed easier to occur during liquefaction; the opposing current makes the fine sand seabed more difficult to be liquefied.

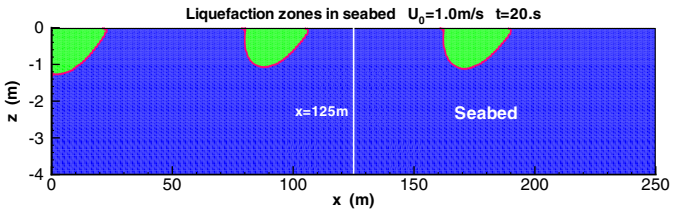

Fig. 16. Liquefaction zones in the seabed (fine sand) under nonlinear wave loading at time $t = 20.0$ s ($H = 3.0$ m, $d = 10.0$ m, $T = 8.0$ s, $U_0 = 1$ m/s)

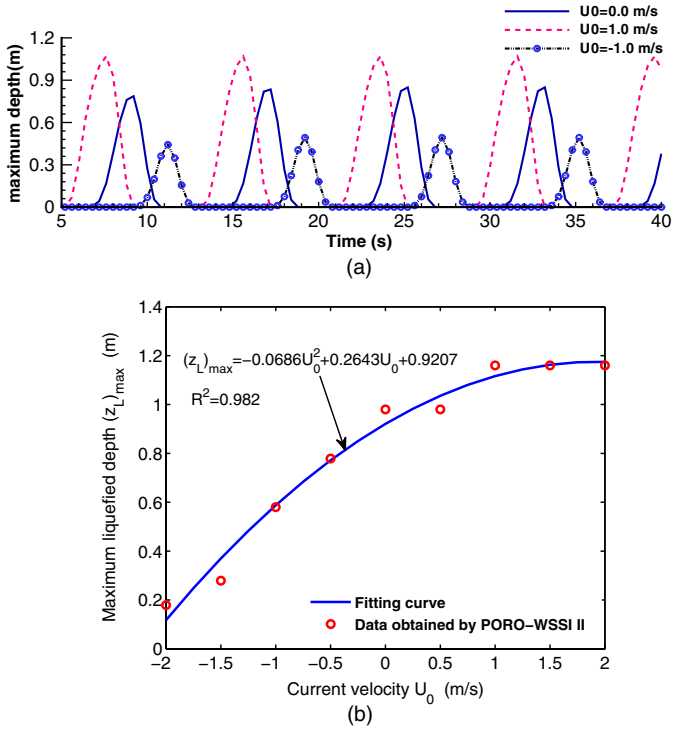

Fig. 17. (a) The variation process of the liquefied depth in the seabed (fine sand) at $x = 125$ m under a nonlinear wave and different current loading; (b) the wave-current induced maximum liquefied depth in the seabed (fine sand) at $x = 125$ m versus different current velocity U_0, and the fitting curve ($H = 3.0$ m, $d = 10.0$ m, $T = 8.0$ s)

Conclusions

The effect of an ocean current, which generally exists simultaneously with an ocean wave, on the seabed response under third-order nonlinear wave and current loading are investigated by adopting the $u - p$ approximation and poroelastic model. The FEM is used to solve the boundary value problem. Based on the numerical analysis presented, the following conclusions can be drawn.

- The following current in a nonlinear wave field makes the seabed response, including pore pressure, effective stresses, shear stress, become greater than without currents in both coarse and fine sand. On the other hand, the opposing current makes the seabed response become smaller than when there is no current both in coarse and fine sand. For example, the following current $U_0 = 1$ m/s makes the maximum relative difference of pore pressure, σ'_x, σ'_z, and shear stress τ_{xz} reach up to 8%, 10%, 5%, and 7% in coarse sand, respectively. The opposing current $U_0 = -1$ m/s makes the maximum relative differences reach up to -10%, -9.5%, -7%, and -10% in coarse sand, respectively. The exclusion of the following current will result in the underestimation of the wave-induced seabed response.
- It is found that the following current makes the seabed more likely to be liquefied, while the opposing current is beneficial to prevent the seabed from liquefaction or shear failure. In the numerical examples, the maximum transient depth in the seabed is 1.16 m, 0.98 m and 0.58 m when $U_0 = 1$ m/s, $U_0 = 0$ m/s, and $U_0 = -1$ m/s, respectively. The qualitative relationship between the maximum liquefaction depth and current velocity is $(z)_{\max} = -0.0868U_0^2 + 0.2643U_0 + 0.9207$. Therefore, the exclusion of the following current will directly lead to the underestimation of the liquefaction depth.

- The magnitude of the current velocity directly determines the effect extent of the current on the seabed response. The greater the current velocity, the more significant the effect of the current on the seabed response. For $U_0 = 2$ m/s, the maximum relative difference of pore pressure is 15%, while it is only 8% when $U_0 = 1$ m/s. For $U_0 = -2$ m/s, the maximum relative difference of the pore pressure is -25%, while it is only -10% when $U_0 = -1$ m/s.
- The parametric study indicates that the wave and seabed characteristics significantly affect the effects of the current on the seabed response under nonlinear wave and current loading. The effect of the current is more obvious for a short period wave propagating in deep water on a saturated seabed compared with a long wave propagating in shallow water on an unsaturated seabed. For example, the maximum relative difference of the pore pressure could reach 25% and 20% for the cases of $T = 5$ s and $d = 15$ m, respectively.

Acknowledgments

We are grateful for the financial support from EPSRC Grant #EP/G006482/1 (UK), State Key Laboratory of Ocean Engineering Self-Development Grant #GKZD010053 (China), Sichuan University State Key Laboratory of Hydraulics and Mountain River Engineering Open Fund Scheme #SKLH-OF-1005(China), and NSFC Grant # 41176073 (China).

References

Baddour, R. E., and Song, S. W. (1990a). "Interaction of higher-order water waves with uniform currents." *Ocean Eng.*, 17(6), 551–568.

Baddour, R. E., and Song, S. W. (1990b). "On the interaction between waves and currents." *Ocean Eng.*, 17(1–2), 1–21.

Biot, M. A. (1941). "General theory of three-dimensional consolidation." *J. Appl. Phys.*, 12(2), 155–164.

Biot, M. A. (1956). "Theory of propagation of elastic waves in a fluidsaturated porous solid, part I: Low frequency range." *J. Acoust. Soc. Am.*, 28(2), 168–177.

Chan, A. H. C. (1988). "A unified finite element solution to static and dynamic problems of geomechanics." Ph.D. thesis, Univ. of Wales, Swansea, Wales.

Esrig, M. I., and Kirby, R. C. (1977). "Implication of gas content for predicting the stability of submarine slopes." *Marine Geotechnol.*, 2(1–4), 81–100.

Hsu, H. C., Chen, Y. Y., Hsu, J. R. C., and Tseng, W. J. (2009). "Nonlinear water waves on uniform current in lagrangian coordinates." *J. Nonlinear Math. Phys.*, 16(1), 47–61.

Hsu, J. R. C., and Jeng, D.-S. (1994). "Wave-induced soil response in an unsaturated anisotropic seabed of finite thickness." *Int. J. Numer. Anal. Methods Geomech.*, 18(11), 785–807.

Hsu, J. R. C., Tsuchiya, Y. Y., and Silvester, R. (1979). "Third-order approximation to short-crested waves." *J. Fluid Mech.*, 90(01), 179–196.

Jeng, D.-S. (2001). "A new wave dispersion equation: Effects of soil characteristics." *J. Offshore Mech. Arctic Eng.*, 123(4), 177–181.

Jeng, D.-S. (2003). "Wave-induced sea floor dynamics." *Appl. Mech. Rev.*, 56(4), 407–429.

Jeng, D.-S., and Cha, D. H. (2003). "Effects of dynamic soil behavior and wave non-linearity on the wave-induced pore pressure and effective stresses in porous seabed." *Ocean Eng.*, 30(16), 2065–2089.

Jeng, D.-S., Cha, D. H., Lin, Y. S., and Hu, P. S. (2000). "Analysis on pore pressure in an anisotropic seabed in the vicinity of a caisson." *Appl. Ocean Res.*, 22(6), 317–329.

Jeng, D.-S., and Lin, Y. S. (1996). "Finite element modelling for water waves–soil interaction." *Soil Dyn. Earthquake Eng.*, 15(5), 283–300.

Jeng, D.-S., and Ou, J. (2010). "3-d models for wave-induced pore pressure near breakwater heads." *Acta Mech.*, 215(1–4), 85–104.

Jeng, D.-S., Rahman, M. S., and Lee, T. L. (1999). "Effects of inertia forces on wave-induced seabed response." *Int. J. Offshore Polar Eng.*, 9(4), 307–313.

Jian, Y. J., Zhu, Q. Y., Zhang, J., and Wang, Y. F. (2009). "Third order approximation to capillary gravity short crested waves with uniform currents." *Appl. Math. Modell.*, 33(4), 2035–2053.

Lu, H. B. (2005). "The research on pore water pressure response to waves in sandy seabed." Ph.D. thesis, Changsha Univ. of Science & Technology, Changsha, China.

Lundgren, H., Lindhardt, J. H. C., and Romold, C. J. (1989). "Stability of breakwaters on porous foundation." *Proc., 12th Int. Conf. on Soil Mech. and Foundation Eng.*, Vol. 1, 451–454.

Okusa, S. (1985). "Wave-induced stress in unsaturated submarine sediments." *Geotechnique*, 35(4), 517–532.

Pietruszczak, S., and Pande, G. N. (1996). "Constitutive relations for partially saturated soils containing gas inclusions." *J. Geotech. Eng.*, 122(1), 50–59.

Thomas, G. P. (1981). "Wave-current interactions: An experimental and numerical study. Part I. Linear waves." *J. Fluid Mech.*, 110, 457–474.

Thomas, S. D. (1989). "A finite element model for the analysis of wave induced stresses, displacements and pore pressure in an unsaturated seabed. I: Theory." *Comput. Geotech.*, 8(1), 1–38.

Thomas, S. D. (1995). "A finite element model for the analysis of wave induced stresses, displacements and pore pressure in an unsaturated seabed. II: Model verification." *Comput. Geotech.*, 17(1), 107–132.

Ulker, M. B. C., Rahman, M. S., and Jeng, D.-S. (2009). "Wave-induced response of seabed: Various formulations and their applicability." *Appl. Ocean Res.*, 31(1), 12–24.

Yamamoto, T., Koning, H., Sellmeijer, H., and Hijum, E. V. (1978). "On the response of a poro-elastic bed to water waves." *J. Fluid Mech.*, 87(1), 193–206.

Zen, K., Umehara, Y., and Finn, W. D. L. (1985). "A case study of the wave-induced liquefaction of sand layers under damaged breakwater." *Proc., 3rd Canadian Conf. on Marine Geotech. Eng.*, Canadian Geotechnical Society, Richmond, BC, Canada, 505–520.

Zienkiewicz, O. C., Chang, C. T., and Bettess, P. (1980). "Drained, undrained, consolidating and dynamic behaviour assumptions in soils." *Geotechnique*, 30(4), 385–395.

Zienkiewicz, O. C., and Scott, F. C. (1972). "On the principle of repeatability and its application in analysis of turbine and pump impellers." *Int. J. Numer. Methods Eng.*, 4(3), 445–452.